Finite Element Analysis of Concrete Structures Using Plastic-Damage Model in 3-D Implementation

O. Omidi[1] and V. Lotfi[2,*]

Received: October 2009 Accepted: August 2010

Abstract: *Neither damage mechanics model nor elastoplastic constitutive law can solely describe the behavior of concrete satisfactorily. In fact, they both fail to represent proper unloading slopes during cyclic loading. To overcome the disadvantages of pure plastic models and pure damage approaches, the combined effects need to be considered. In this regard, various classes of plastic-damage models have been recently proposed. Here, the theoretical basics of the plastic-damage model originally proposed by Lubliner et al. and later on modified by Lee and Fenves is initially presented and its numerical aspects in three-dimensional space are subsequently emphasized. It should be mentioned that a part of the implementation in 3-D space needs to be reformulated due to employing a hyperbolic potential function to treat the singularity of the original linear form of plastic flow proposed by Lee and Fenves. The consistent algorithmic tangent stiffness, which is utilized to accelerate the convergence rate in solving the nonlinear global equations, is also derived. The validation and evaluation of the model to capture the desired behavior under monotonic and cyclic loadings are shown with several simple one-element tests. These basic simulations confirm the robustness, accuracy, and efficiency of the algorithm at the local and global levels. At the end, a four-point bending test is examined to demonstrate the capabilities of the model in real 3-D applications.*

Keywords: *plastic-damage; cyclic loading; consistent algorithmic tangent stiffness; numerical implementation; concrete model; plasticity theory*

1. Introduction

There have been significant efforts in computational mechanics to describe the behavior of concrete using various proposed models. As the softening zone is known to result from the formation of microcracks, the strain softening is one of the most important aspects of concrete behavior. As well as the hardening behavior which occurs under compressive loading, a constitutive model for concrete materials should represent the softening behavior correctly. The stiffness degradation is another important issue to simulate the crack opening and closing under cyclic loading.

The cracking process in concrete can be categorized into several approaches including discrete crack, smeared crack, damage mechanics and plasticity-based models. Among different versions of plasticity-based models, the plastic-damage constitutive law is a suitable approach to simulate concrete behavior due to its capabilities of including not only inelastic strain but also stiffness degradation. It is well recognized that cracking reduces the stiffness of concrete structural components. Therefore, in order to accurately model the degradation in the mechanical properties of concrete, the use of continuum damage mechanics is necessary. However, the concrete material also experiences some irreversible deformations during unloading such that the continuum damage theories cannot be used alone. Therefore, the nonlinear material behavior of concrete can be precisely simulated by two separate material mechanical processes: damage and plasticity.

Plasticity theory has been widely used alone to describe the concrete behavior [1-4]. The main characteristic of these models is a plasticity yield surface that includes pressure sensitivity, path sensitivity, non-associative flow rule, and work or strain hardening. However, such models failed to address the degradation of the material stiffness due to micro-cracking. On the other

* *Corresponding Author: Email: vahlotfi@aut.ac.ir*

1 PhD Candidate of Structural Eng., Civil and Environmental Eng. Department, Amirkabir University of Technology, Tehran, Iran.

2 Professor of Structural Eng., Civil and Environmental Eng. Department, Amirkabir University of Technology, Tehran, Iran.

[Downloaded from ijce.iust.ac.ir on 2026-11-11]

hand, the continuum damage theory has been also employed alone to model the material nonlinear behavior such that the mechanical effects of the progressive micro-cracking and strain softening are represented by a set of internal variables which act on the elastic behavior (i.e. decrease of the stiffness) at the macroscopic level [5-7]. Furthermore, concrete behavior has several aspects such as irreversible deformations, inelastic volumetric expansion in compression, and crack opening/closure effects that cannot be represented by the two above-mentioned methods alone. Since both micro-cracking and irreversible deformations are contributing to the nonlinear response of concrete, a constitutive model should address equally the two physically distinct modes of irreversible changes.

Combinations of plasticity and damage are usually based on isotropic hardening combined with either isotropic (scalar) damage or anisotropic (tensor) damage. Isotropic damage is widely used due to its simplicity such that different types of combinations with plasticity models have been proposed in the literature. There are two approaches for this combination. One relies on stress-based plasticity formulated in the effective (undamaged) space [8-11] and another alternative is founded on stress-based plasticity in the nominal (damaged) stress space [12,13]. However, the coupled plastic-damage models formulated in the effective space are numerically more stable and attractive [9,14].

The purpose of this paper is to discuss computational issues involved in the modeling of plain concrete in view of an approach which takes advantages of both plasticity and damage mechanics alternatives. The model referred to as plastic-damage in literature employs two internal variables as the damage parameters in tension and compression separately. This constitutive model was originally proposed by Lubliner et al. [12] and later modified by Lee and Fenves [15]. It is also worthwhile to mention that in this latter study, computational aspects of the 3-D formulation are also briefly presented along with the more complete 2-D examples with plane stress behavior from numerical implementation point of view. In 3-D space, the process of return-mapping needs to be reformulated due to employing a hyperbolic potential function to treat the singularity of the original linear form of plastic flow proposed by Lee and Fenves. In the present study, the details of 3-D implementation of the model are discussed. Moreover, a special finite element program is developed in that context which is generally ideal for three dimensional nonlinear analyses of concrete structures under cyclic loading. It should be added that in the present work, the rate-independent plasticity and the isotropic continuum damage mechanics theories are applied to the elastic and inelastic constitutive laws. Additionally, the infinitesimal deformation theory, which is reasonable and adequate for concrete, is assumed as well.

An outline of the remainder of this paper is as follows: In Section 2, the framework of the plastic-damage model is summarized. It includes the basic concepts emphasizing on uniaxial state in tension and compression and then multiaxial behavior. This section is followed by introducing the stiffness degradation which plays an important role in cyclic loading states. The yield and potential functions utilized in the study are introduced at the end of this section. In the next section, the computational issues involved in the numerical integration of the model are discussed. Section 3 also presents the procedure used for the stress calculation of each Gauss point within global iterations. Moreover, the algorithmic tangent stiffness which accelerates the convergence rate in the nonlinear global solution is formulated in that part. Finally in Section 4, some numerical simulations including several one-element validation tests and two real applications are presented to demonstrate different features of the model and to establish comparisons with some available experimental data.

2. Theoretical Basics of Plastic-Damage Model

Based on the incremental theory of plasticity, the strain tensor, $\boldsymbol{\varepsilon}$, is decomposed into the elastic part, $\boldsymbol{\varepsilon}^{e}$, and the plastic part, $\boldsymbol{\varepsilon}^{p}$:

$$\boldsymbol{\varepsilon} = \boldsymbol{\varepsilon}^{e} + \boldsymbol{\varepsilon}^{p} \tag{1}$$

[Downloaded from ijce.iust.ac.ir on 2026-11-11]

The elastic part is defined as the recoverable portion in the total strain, which for linear elasticity, is given by:

$$\boldsymbol{\varepsilon}^{\mathrm{e}} = \mathbf{E}^{-1} : \boldsymbol{\sigma} \tag{2}$$

where the elastic stiffness, **E**, is a rank four tensor, and $\boldsymbol{\sigma}$ is the stress tensor. Based on equations (1) and (2), the stress and strain relation can be written as:

$$\boldsymbol{\sigma} = \mathbf{E} : (\boldsymbol{\varepsilon} - \boldsymbol{\varepsilon}^{\mathrm{p}}) \tag{3}$$

If scalar damage in stiffness degradation is assumed, the elastic stiffness is defined as:

$$\mathbf{E} = (1 - D)\,\mathbf{E}_0 \tag{4}$$

where D is the degradation variable and $\mathbf{E_0}$ is the initial stiffness tensor. Substituting equation (4) into equation (3) leads to the following relation:

$$\boldsymbol{\sigma} = (1 - D)\,\mathbf{E}_0 : (\boldsymbol{\varepsilon} - \boldsymbol{\varepsilon}^{\mathrm{p}}) \tag{5}$$

This equation may also be written as:

$$\boldsymbol{\sigma} = (1 - D)\,\bar{\boldsymbol{\sigma}} \tag{6}$$

where $\bar{\sigma}$ is denoted as the effective stress, given as:

$$\bar{\boldsymbol{\sigma}} = \mathbf{E}_0 : (\boldsymbol{\varepsilon} - \boldsymbol{\varepsilon}^{\mathrm{p}}) \tag{7}$$

According to equation (6), the constitutive relation for elastoplastic response is decoupled from the degradation damage response, which provides advantages in the numerical implementation. Therefore, the strength function for the effective stress is used in this model to control the evolution of the yield surface, such that calibration with experimental results becomes convenient.

The plastic strain rate, which is evaluated by a flow rule, is assumed to be related to a scalar potential function Φ. For a plastic potential defined in the effective-stress space, it is given by:

$$\dot{\boldsymbol{\varepsilon}}^{\mathrm{p}} = \dot{\lambda}\,\nabla_{\bar{\boldsymbol{\sigma}}}\Phi \tag{8}$$

where $\nabla_{\bar{\boldsymbol{\sigma}}}\Phi = \partial\Phi / \partial\bar{\boldsymbol{\sigma}}$ and λ is a nonnegative function referred to as the plastic consistency parameter. In addition to the plastic strain, another internal variable set is required to represent the damage states. Consequently, it is assumed that the plastic-damage variable **k** is the only necessary state variable and its evolution is expressed as:

$$\dot{\boldsymbol{\kappa}} = \dot{\lambda}\,\mathbf{H}(\bar{\boldsymbol{\sigma}}, \boldsymbol{\kappa}) \tag{9}$$

As shown later, the function **H** can be derived considering plastic dissipation. At this stage, uniaxial behavior of concrete is initially considered for tension and compression in order to describe the basic concepts of the model. Subsequently, this is extended to multiaxial states under complex loading utilized for a general 3-D implementation.

2.1. Definition of Damage Variables

The model utilizes two damage variables to represent tensile and compressive damage independently, which is required to simulate concrete behavior under cyclic loading. These damage variables would have values within the range of zero to one. Considering a uniaxial state of stress, the state variable $\aleph \in \{\mathrm{t}, \mathrm{c}\}$ is introduced. In that respect, tension and compression states are denoted by $\aleph = \mathrm{t}$ and $\aleph = \mathrm{c}$, respectively. Accordingly, each uniaxial strength function is expressed in terms of its corresponding plastic-damage parameter, $\mathrm{k}_{\aleph}$. In the Barcelona model (i.e., initial form of the plastic-damage model) which was originally proposed by Lubliner and co-authors [12], the uniaxial stress is assumed to be related to the scalar plastic strain variable symbolized by ε^{p}:

$$\begin{aligned} \sigma_{\aleph} &= f_{\aleph}(\varepsilon^{\mathrm{p}}) \\ &= f_{\aleph 0}\left[(1 + a_{\aleph})\exp(-b_{\aleph}\varepsilon^{\mathrm{p}}) - a_{\aleph}\exp(-2\,b_{\aleph}\varepsilon^{\mathrm{p}})\right] \end{aligned} \tag{10}$$

where $a_{\aleph}$, $b_{\aleph}$ are constants, and $f_{\aleph 0}$ is the initial yield stress, defined as the maximum stress without damage. The above strength function is assumed to be factorized as:

$$\sigma_{\aleph} = (1 - D_{\aleph})\,\bar{\sigma}_{\aleph} \tag{11}$$

[Downloaded from ijce.iust.ac.ir on 2026-11-11]

In this relation, $D_{\aleph}$ and $\bar{\sigma}_{\aleph}$ are defined as the degradation damage variable and the effective stress response for the uniaxial state $\aleph$, respectively. It should be mentioned that the degradation damage variables are also defined as increasing functions of plastic-damage variables. They can take values from zero, corresponding to the undamaged concrete, up to one, which represents fully damaged concrete. An exponential form is normally assumed for the degradation, $D_{\aleph}$, as below:

$$1 - D_{\aleph} = \exp(-c_{\aleph}\varepsilon^{p}) \tag{12}$$

where $c_{\aleph}$ is a constant. Thus, the effective stress can be written as follows based on equations (10), (11) and (12):

$$\begin{aligned}\bar{\sigma}_{\aleph} &= \bar{f}_{\aleph}(\varepsilon^{p}) \\ &= f_{\aleph 0}\left[(1+a_{\aleph})\left(\exp(-b_{\aleph}\varepsilon^{p})\right)^{1-\frac{c_{\aleph}}{b_{\aleph}}} - a_{\aleph}\left(\exp(-b_{\aleph}\varepsilon^{p})\right)^{2-\frac{c_{\aleph}}{b_{\aleph}}}\right]\end{aligned} \tag{13}$$

The uniaxial stress curves are illustrated in Fig. 1. It is noted in these diagrams that total strain is decomposed into two parts, the elastic strain $\boldsymbol{\varepsilon}^{e}$ and the plastic part ε^{p}.

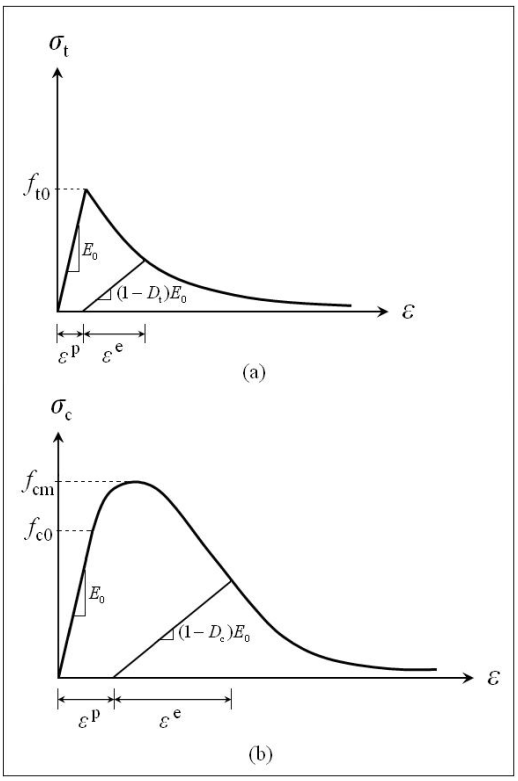

Fig. 1. Uniaxial local curves : (a) in tension, (b) in compression

Furthermore, the plastic-damage variables in tension and compression are defined based on the following relations [12,15]:

$$\kappa_{\aleph} = \frac{1}{g_{\aleph}}\int_{0}^{\varepsilon^{p}} \sigma_{\aleph}\, d\varepsilon^{p} \;;\; g_{\aleph} = \int_{0}^{\infty} \sigma_{\aleph}\, d\varepsilon^{p} \tag{14}$$

where $g_{\aleph}$ is the specific fracture energy, defined as the fracture energy normalized by the localization size zone, also referred to as the characteristic length, $l_{\aleph}$ (i.e., $g_{\aleph} = G_{\aleph} / I_{\aleph}$). It is noted that $0 \le \kappa_{\aleph} \le 1$.

Substituting Eq. (10) into Eq. (14) yields the relation between $k_{\aleph}$ and $\boldsymbol{\varepsilon}^{p}$, which can be substituted back into equation (10) to express the uniaxial stress in terms of $k_{\aleph}$, i.e., $\sigma_{\aleph} = f_{\aleph}(\kappa_{\aleph})$. Similarly, the effective stress and degradation damage variables can be stated in terms of $\boldsymbol{k}_{\aleph}$ as $\bar{\sigma}_{\aleph} = \bar{f}_{\aleph}(\kappa_{\aleph})$ and $D_{\aleph} = D(\kappa_{\aleph})$, respectively. It is also worthwhile to mention that the parameters utilized in equation (13) (i.e., $a_{\aleph}$, $b_{\aleph}$ and $c_{\aleph}$) could be determined by employing the usual parameters defined in Fig. 1, as well as some additional enforced values of tensile degradation at $\sigma_t = 0.5 f_{t0}$ (i.e., $\tilde{D}_t$) and compressive degradation at $\sigma_c = f_{cm}$ (i.e., $\tilde{D}_c$) [9,15].

2.2. Damage Evolution in Multiaxial Behavior

By utilizing Eqs (10) and (14), the damage evolution equation for the uniaxial state can be written as [9]:

$$\dot{\kappa}_{\aleph} = \frac{1}{g_{\aleph}} f_{\aleph}(\kappa_{\aleph})\,\dot{\varepsilon}^{p} \tag{15}$$

To extend the uniaxial version of damage evolution equation to the multi-dimensional case, the scalar plastic strain rate $\dot{\varepsilon}^{p}$ in Eq. (15) is assumed to be evaluated in the general three-dimensional case by the following relation:

$$\dot{\varepsilon}^{p} = \delta_{t\aleph}\, r(\hat{\bar{\boldsymbol{\sigma}}})\,\dot{\hat{\varepsilon}}^{p}_{max} + \delta_{c\aleph}\,(1 - r(\hat{\bar{\boldsymbol{\sigma}}}))\,\dot{\hat{\varepsilon}}^{p}_{min} \tag{16}$$

where δ is Kronecker delta and $\dot{\hat{\varepsilon}}^{p}_{max}$, $\dot{\hat{\varepsilon}}^{p}_{min}$, are the algebraically maximum and minimum eigenvalues of rate of the plastic strain tensor, respectively. The scalar quantity $r(\hat{\bar{\boldsymbol{\sigma}}})$ is a weight

[Downloaded from ijce.iust.ac.ir on 2026-11-11]

factor, which is within the range zero to one. Denoting the ramp function as $\langle x\rangle = (x+|x|)/2$, $r(\hat{\bar{\boldsymbol{\sigma}}})$ is defined by:

$$r(\hat{\bar{\boldsymbol{\sigma}}}) = \left(\sum_{i=1}^{3}\langle\hat{\bar{\sigma}}_i\rangle\right) \Big/ \left(\sum_{i=1}^{3}|\hat{\bar{\sigma}}_i|\right) \tag{17}$$

As two plastic-damage variables are independently used in tension and compression, the plastic-damage vector is defined as $\boldsymbol{\kappa} = (\kappa_t \quad \kappa_c)^T$. Substitution of eq. (16) into eq. (15) results in an evolution equation for the general case in the form of:

$$\dot{\boldsymbol{\kappa}} = \mathbf{h}(\hat{\bar{\boldsymbol{\sigma}}}, \boldsymbol{\kappa}) : \hat{\dot{\boldsymbol{\varepsilon}}}^p \tag{18}$$

where **h** in matrix notation is written as:

$$\mathbf{h}(\hat{\bar{\boldsymbol{\sigma}}}, \boldsymbol{\kappa}) = \begin{pmatrix} \dfrac{r(\hat{\bar{\boldsymbol{\sigma}}})}{g_t} f_t(\kappa_t) & 0 \\ 0 & \dfrac{(1-r(\hat{\bar{\boldsymbol{\sigma}}}))}{g_c} f_c(\kappa_c) \end{pmatrix} \tag{19}$$

Furthermore, the flow rule in eq. (8) can be modified into one for $\hat{\dot{\boldsymbol{\varepsilon}}}^p$:

$$\hat{\dot{\boldsymbol{\varepsilon}}}^p = \dot{\lambda} \nabla_{\hat{\bar{\boldsymbol{\sigma}}}} \hat{\Phi} \tag{20}$$

By substituting Eq. (20) into Eq. (18), the damage evolution equation can be written as:

$$\dot{\boldsymbol{\kappa}} = \dot{\lambda}\, \mathbf{H}(\hat{\bar{\boldsymbol{\sigma}}}, \boldsymbol{\kappa}) \; ; \quad \mathbf{H} = \mathbf{h} : \nabla_{\hat{\bar{\boldsymbol{\sigma}}}} \hat{\Phi} \tag{21}$$

2.3. Stiffness Degradation

The degradation of stiffness, which is caused by microcracking, occurs in both tension and compression and becomes more significant as the strain increases. Under cyclic loading, the mechanism of stiffness degradation gets more complicated due to opening and closing of the microcracks. Since the scalar degradation, which is assumed to depend on only *k*, is considered in the present study, exact simulation of the complicated degradation phenomena is very difficult. As the model is accurately capable of capturing two major damage phenomena, the uniaxial tensile and compressive ones, degradation in multi-dimensional behavior can be possibly evaluated by interpolating between these two main degradation damages such as:

$$D = 1 - (1 - D_c(\kappa_c))\,(1 - D_t(\kappa_t)) \tag{22}$$

Where both D_t and D_c are defined in equation (12). Eq. (22) does not capture the correct crack opening/closing behavior, which can be implemented by elastic stiffness recovery during elastic unloading process from tensile state to compressive state. Thus, D is modified by multiplying the tensile degradation in eq. (22) by a parameter which is a function of the stress state, $s(\hat{\bar{\boldsymbol{\sigma}}})$:

$$D = 1 - (1 - D_c)\,(1 - s(\hat{\bar{\boldsymbol{\sigma}}})\, D_t) \tag{23}$$

where $0 \le s \le 1$ and is referred to as the stiffness recovery factor. A possible form of ***s*** is:

$$s(\hat{\bar{\boldsymbol{\sigma}}}) = s_0 + (1 - s_0)\, r(\hat{\bar{\boldsymbol{\sigma}}}) \tag{24}$$

in which r is defined in Eq. (17) and s_0 is a constant to set the minimum value of s [9]. It is also apparent that $r(\hat{\boldsymbol{\sigma}}) = r(\hat{\bar{\boldsymbol{\sigma}}})$ due to scalar degradation assumption.

2.4. Yield Surface

Since concrete behaves differently in tension and compression, the plasticity yield criterion cannot be assumed to be alike. Considering the same yield surface for both tension and compression in concrete materials can lead to over/under estimate of plastic deformation [12,15]. The Mohr-Coulomb criterion is the most well-known yield function for frictional materials such as concrete. In this model, the J_3 term is included to make the yield surface more realistic. In Lubliner's model, the algebraically largest principal stress is used instead of J_3 [12]. This is also adopted in the present study. The yield surface is expressed here in terms of effective stress tensor and the plastic-damage variables as:

$$F(\bar{\boldsymbol{\sigma}}, \boldsymbol{\kappa}) = \frac{1}{1-\alpha}\Big[\alpha \bar{I}_1 + \sqrt{3\bar{J}_2} + \beta(\boldsymbol{\kappa})\langle\hat{\bar{\sigma}}_{max}\rangle - \gamma\langle -\hat{\bar{\sigma}}_{max}\rangle\Big] - c_c(\boldsymbol{\kappa}) \tag{25}$$

where parameters $\bar{I}_1$ and $\bar{J}_2$ are the first and second invariants of the effective stress tensor.

[Downloaded from ijce.iust.ac.ir on 2026-11-11]

The maximum principal stress is also denoted by $\hat{\bar{\boldsymbol{\sigma}}}_{n+1}$. Moreover, a is a dimensionless constant and it depends on the ratio of yield strengths under biaxial and uniaxial compression, (i.e., f_{b0}/f_{c0}):

$$\alpha = \frac{(f_{b0}/f_{c0})-1}{2(f_{b0}/f_{c0})-1} \tag{26}$$

Originally, Lublinear et al. presented β and γ as constant parameters [12]. However, Lee and Fenves [9] later modified β as a dimensionless variable which is written as a function of the two plastic-damage parameters, k_t and k_c :

$$\beta(\boldsymbol{\kappa}) = \frac{c_c(\kappa_c)}{c_t(\kappa_t)}(1-\alpha)-(1+\alpha)\ ;\ \ \gamma = \frac{3(1-\rho_c)}{2\rho_c-1} \tag{27}$$

where c_t and c_c ,which are equal to $\bar{f}_t(\kappa_t)$ and $\bar{f}_c(\kappa_c)$, denote the effective tensile and compressive cohesions (positive values utilized here), respectively. Moreover, ρ_c is the ratio of corresponding values of $\sqrt{\bar{J}_2}$ for tensile and compressive axes at any given value of the hydrostatic pressure, $\bar{I}_1$. It is usually assumed as a constant, with a typical value of 2/3 for concrete [12], which results in the value of γ=3. Since the influence of coefficient γ disappears in stress states other than triaxial compression (i.e., $\hat{\bar{\sigma}}_{max} < 0$), the corresponding term in Eq. (25) can be viewed as a minor modification to improve the predictive capability of the model under stress states other than the plane stress conditions. Moreover, the yield surface can be represented alternatively as $F(\bar{\boldsymbol{\sigma}},\boldsymbol{\kappa}) = \hat{F}(\hat{\bar{\boldsymbol{\sigma}}},\boldsymbol{\kappa})$ [16].

2. 5. Plastic Potential Function

The non-associative plasticity flow rule, which is important for realistic modeling of the volumetric expansion under compression for frictional materials such as concrete, is employed here. The Drucker-Prager linear function was utilized by Lee and Fenves in their 2-D studies [9,16] as the potential flow:

$$\Phi(\bar{\boldsymbol{\sigma}}) = \sqrt{2\bar{J}_2} + \alpha_p \bar{I}_1 \tag{28}$$

where the parameter a_p should be calibrated to give proper dilatancy [9]. It is well-known that this type of surface has a singularity at the apex. Although this will not cause any difficulty for the plane stress 2-D condition considered by Lee and Fenves [9], it would be problematic for the 3-D implementation of the present study and it requires special attention. The strategy chosen herein is to employ the Drucker-Prager hyperbolic function as equation (29) which has been depicted in Fig. 2 as well.

$$\Phi(\bar{\boldsymbol{\sigma}}) = \sqrt{\beta_H^2 + 2\bar{J}_2} + \alpha_p \bar{I}_1\ ;\ \ \beta_H = \varepsilon_1 \alpha_p f_{t0} \tag{29}$$

where $\boldsymbol{\varepsilon}_1$ is a parameter which adjusts how the flow potential approaches its corresponding linear function. Since the hyperbolic function is continuous and smooth, the flow direction is always uniquely defined.

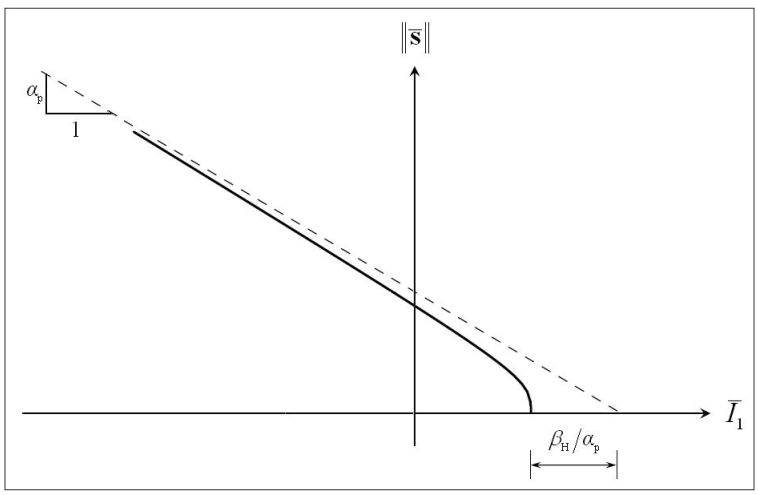

Fig. 2. Drucker-Prager hyperbolic function along with its asymptote in the meridian plane

[Downloaded from ijce.iust.ac.ir on 2026-11-11]

3. Numerical Implementation

3.1. Linearization of Damage Evolution Equations

The damage evolution equation (i.e., Eq. (21)) can be expressed in discrete form based on the backward-Euler method:

$$\Delta\boldsymbol{\kappa} = \Delta\lambda\,\mathbf{H}(\hat{\bar{\boldsymbol{\sigma}}}_{n+1}, \boldsymbol{\kappa}_{n+1}) \tag{30}$$

This may also be rewritten as:

$$\boldsymbol{\kappa}_{n+1} = \boldsymbol{\kappa}_n + \lambda\,\mathbf{H}(\hat{\bar{\boldsymbol{\sigma}}}_{n+1}, \boldsymbol{\kappa}_{n+1}) \tag{31}$$

where λ is used instead of $\Delta\lambda$ for simplicity. Since the above equation is a nonlinear relation, an iterative solution scheme for the effective stress, **k** and λ is required to be carried out (this is referred to as the local iteration). For this purpose, the Newton-Raphson approach is utilized here [9]. The residual for Eq. (31) denoted by **Q** is:

$$\mathbf{Q}(\hat{\bar{\boldsymbol{\sigma}}}_{n+1}, \boldsymbol{\kappa}_{n+1}, \lambda) = -\boldsymbol{\kappa}_{n+1} + \boldsymbol{\kappa}_n + \lambda\,\mathbf{H}(\hat{\bar{\boldsymbol{\sigma}}}_{n+1}, \boldsymbol{\kappa}_{n+1}) \tag{32}$$

This residual equation, which needs to be satisfied (i.e.,**Q**=0), is iterated using the Newton-Raphson scheme as:

$$\left(\frac{d\mathbf{Q}}{d\boldsymbol{\kappa}}\right)^{(j)}_{n+1} \delta\boldsymbol{\kappa} = -\,\mathbf{Q}^{(j)}_{n+1} \tag{33}$$

in which $d\mathbf{Q}$ / $d\mathbf{k}$ is the Jacobian matrix and $\delta\boldsymbol{\kappa}$ is used to update the plastic-damage vector, $\mathbf{k}_{n+1}$:

$$\boldsymbol{\kappa}^{(j+1)}_{n+1} = \boldsymbol{\kappa}^{(j)}_{n+1} + \delta\boldsymbol{\kappa} \tag{34}$$

The local iteration scheme, which actually plays the role of the return-mapping process in this model, is summarized in Table 1. The required formulas to compute λ and $\hat{\bar{\boldsymbol{\sigma}}}_{n+1}$ that are employed in this procedure will be derived in the following sections.

3.2. Stress Computation

From a numerical point of view, the nonlinear behavior of concrete model may be treated as an implicit time discrete strain-driven problem. Accordingly, the time discrete equations of the model are integrated over a time interval $(t_n, t_{n+1} = t_n + \Delta t)$ using an implicit backward-Euler scheme, which is unconditionally stable [16,17]. The stress and the plastic strain at step $n+1$ are expressed as:

$$\boldsymbol{\sigma}_{n+1} = \boldsymbol{\sigma}_n + \Delta\boldsymbol{\sigma}\ ; \quad \boldsymbol{\varepsilon}^{\mathrm{p}}_{n+1} = \boldsymbol{\varepsilon}^{\mathrm{p}}_n + \Delta\boldsymbol{\varepsilon}^{\mathrm{p}} \tag{35}$$

From Eq. (6), the stress can be written in the following form:

$$\boldsymbol{\sigma}_{n+1} = (1 - D_{n+1})\,\bar{\boldsymbol{\sigma}}_{n+1} \tag{36}$$

Moreover, based on Eq. (7), the effective stress becomes:

$$\begin{aligned} \bar{\boldsymbol{\sigma}}_{n+1} &= \mathbf{E}_0 : (\boldsymbol{\varepsilon}_{n+1} - \boldsymbol{\varepsilon}^{\mathrm{p}}_{n+1}) \\ &= \bar{\boldsymbol{\sigma}}^{\mathrm{tr}}_{n+1} - \mathbf{E}_0 : \Delta\boldsymbol{\varepsilon}^{\mathrm{p}} \\ &= \bar{\boldsymbol{\sigma}}^{\mathrm{tr}}_{n+1} - (2\,G_0\Delta\mathbf{e}^{\mathrm{p}} + K_0\Delta\theta^{\mathrm{p}}\mathbf{I}) \end{aligned} \tag{37}$$

where the trial effective stress, denoted by $\bar{\boldsymbol{\sigma}}^{\mathrm{tr}}_{n+1}$, is defined as:

$$\bar{\boldsymbol{\sigma}}^{\mathrm{tr}}_{n+1} = \mathbf{E}_0 : (\boldsymbol{\varepsilon}_{n+1} - \boldsymbol{\varepsilon}^{\mathrm{p}}_n) \tag{38}$$

The above procedure for computation of stress tensor can be interpreted as the three-step predictor-corrector method:

1) Elastic predictor: $\bar{\boldsymbol{\sigma}}^{\mathrm{tr}}_{n+1}$
2) Plastic corrector: $-\mathrm{E}_0$: $\Delta\boldsymbol{\varepsilon}^{\mathrm{p}}$
3) Damage corrector: $-D_{n+1}$ $\bar{\boldsymbol{\sigma}}_{n+1}$

Table 1. Return-mapping process (local iteration)

0. $j = 0$; $\hat{\bar{\boldsymbol{\sigma}}}_{n+1} = \hat{\bar{\boldsymbol{\sigma}}}^{\mathrm{tr}}_{n+1}$; $\boldsymbol{\kappa}^{(0)}_{n+1} = \boldsymbol{\kappa}_n$
1. Obtain λ
2. Compute $\hat{\bar{\boldsymbol{\sigma}}}_{n+1}$
3. $\mathbf{Q}^{(j)}_{n+1} = -\boldsymbol{\kappa}^{(j)}_{n+1} + \boldsymbol{\kappa}_n + \lambda\,\mathbf{H}(\hat{\bar{\boldsymbol{\sigma}}}_{n+1}, \boldsymbol{\kappa}^{(j)}_{n+1})$
4. IF $\left\|\mathbf{Q}^{(j)}_{n+1}\right\| \le Tol_{\mathrm{L}}$ THEN Exit.
5. Form $(d\mathbf{Q}/d\boldsymbol{\kappa})^{(j)}_{n+1}$
6. Solve $\left(\frac{d\mathbf{Q}}{d\boldsymbol{\kappa}}\right)^{(j)}_{n+1} \delta\boldsymbol{\kappa} = -\,\mathbf{Q}^{(j)}_{n+1}$ for $\delta\boldsymbol{\kappa}$
7. $\boldsymbol{\kappa}^{(j+1)}_{n+1} = \boldsymbol{\kappa}^{(j)}_{n+1} + \delta\boldsymbol{\kappa}$
8. $j = j+1$ and GOTO Step 1.

[Downloaded from ijce.iust.ac.ir on 2026-11-11]

The damage part is implemented separately, because it is decoupled from the plastic corrector part. The backward-Euler scheme is used to integrate the plastic strain:

$$\Delta\boldsymbol{\varepsilon}^{\mathrm{p}} = \lambda \nabla_{\bar{\boldsymbol{\sigma}}} \Phi \tag{39}$$

Using the mentioned flow rule, the increment of plastic strain can be rewritten in the split form as:

$$\Delta\boldsymbol{\varepsilon}^{\mathrm{p}} = \Delta\mathbf{e}^{\mathrm{p}} + \frac{\Delta\theta^{\mathrm{p}}}{3}\mathbf{I} \tag{40}$$

$$\Delta\mathbf{e}^{\mathrm{p}} = \lambda \frac{\bar{\mathbf{s}}_{n+1}}{\sqrt{\beta_{\mathrm{H}}^2 + \left\|\bar{\mathbf{s}}_{n+1}\right\|^2}} \;;\quad \Delta\theta^{\mathrm{p}} = 3\,\lambda\,\alpha_{\mathrm{p}} \tag{41}$$

in which, $\bar{\mathbf{s}}$ denotes the deviatoric part of the effective stress and $\|\bar{\mathbf{s}}\| = \sqrt{2\bar{J}_2}$. Moreover, by substituting Eq. (41) into Eq. (37), the effective stress is reformulated as:

$$\bar{\boldsymbol{\sigma}}_{n+1} = \bar{\boldsymbol{\sigma}}^{\mathrm{tr}}_{n+1} - \lambda\left(\frac{2\,G_0\,\bar{\mathbf{s}}_{n+1}}{\sqrt{\beta_{\mathrm{H}}^2 + \left\|\bar{\mathbf{s}}_{n+1}\right\|^2}} + 3K_0\alpha_{\mathrm{p}}\mathbf{I}\right) \tag{42}$$

If the deviatoric and volumetric parts in Eq. (42) are separated and slightly manipulated, the following relations can be concluded:

$$\frac{\bar{\mathbf{s}}_{n+1}}{\left\|\bar{\mathbf{s}}_{n+1}\right\|} = \frac{\bar{\mathbf{s}}^{\mathrm{tr}}_{n+1}}{\left\|\bar{\mathbf{s}}^{\mathrm{tr}}_{n+1}\right\|} \tag{43}$$

$$\left\|\bar{\mathbf{s}}_{n+1}\right\| = \left\|\bar{\mathbf{s}}^{\mathrm{tr}}_{n+1}\right\| - 2\,G_0\lambda\frac{\left\|\bar{\mathbf{s}}_{n+1}\right\|}{\sqrt{\beta_{\mathrm{H}}^2 + \left\|\bar{\mathbf{s}}_{n+1}\right\|^2}} \tag{44}$$

$$(\bar{I}_1)_{n+1} = (\bar{I}_1^{\mathrm{tr}})_{n+1} - 9K_0\lambda\,\alpha_{\mathrm{p}} \tag{45}$$

where $\bar{\mathbf{s}}^{\mathrm{tr}}$ and $\bar{I}_1^{\mathrm{tr}}$ denote the deviatoric part and the first invariant of the trial effective stress, respectively.

When principal stress terms exist in a yield function, the return-mapping algorithm based on a spectral decomposition of the stress is more efficient. This concept is reviewed briefly below and the reader is referred to other references for details [16,17]. It is well known that any symmetric matrix such as the effective stress matrix can be factorized by the spectral decomposition:

$$\bar{\boldsymbol{\sigma}}_{n+1} = \mathbf{P}_{n+1}\,\hat{\bar{\boldsymbol{\sigma}}}_{n+1}\,\mathbf{P}^{\mathrm{T}}_{n+1} \tag{46}$$

where $\mathbf{P}_{n+1}$ is the non-singular matrix whose columns are the orthonormal eigenvectors of $\bar{\sigma}_{n+1}$ and $\hat{\bar{\boldsymbol{\sigma}}}_{n+1}$ is the diagonal matrix of eigenvalues of $\bar{\sigma}_{n+1}$. Moreover, since an isotropic material behavior is assumed, there exists a function $\hat{\Phi}$ such that $\hat{\Phi}(\hat{\bar{\boldsymbol{\sigma}}}) = \Phi(\bar{\boldsymbol{\sigma}})$. Thus, the plastic strain increment, $\Delta\boldsymbol{\varepsilon}^{\mathrm{p}}$, can also be written in the spectral decomposition form [17]:

$$\Delta\boldsymbol{\varepsilon}^{\mathrm{p}} = \lambda\,\mathbf{P}_{n+1}\,\Delta\hat{\boldsymbol{\varepsilon}}^{\mathrm{p}}\,\mathbf{P}^{\mathrm{T}}_{n+1} \;;\quad \Delta\hat{\boldsymbol{\varepsilon}}^{\mathrm{p}} = \lambda\,\nabla_{\hat{\bar{\boldsymbol{\sigma}}}}\hat{\Phi} \tag{47}$$

As proved in [16], any eigenvector of matrix $\bar{\sigma}_{n+1}$ is also an eigenvector of matrix $\bar{\boldsymbol{\sigma}}^{\mathrm{tr}}_{n+1}$, which leads to the spectral decomposition form of $\bar{\boldsymbol{\sigma}}^{\mathrm{tr}}_{n+1}$:

$$\bar{\boldsymbol{\sigma}}^{\mathrm{tr}}_{n+1} = \mathbf{P}_{n+1}\,\hat{\bar{\boldsymbol{\sigma}}}^{\mathrm{tr}}_{n+1}\,\mathbf{P}^{\mathrm{T}}_{n+1} \tag{48}$$

By using the Drucker-Prager hyperbolic plastic function as the flow rule, one can show that by employing the spectral return-mapping briefly discussed above, Eqs. (39) and (42) are written in the context of their eigenvalues as the following, respectively:

$$\Delta\hat{\boldsymbol{\varepsilon}}^{\mathrm{p}} = \lambda\left(\frac{\hat{\bar{\mathbf{s}}}_{n+1}}{\sqrt{\beta_{\mathrm{H}}^2 + \left\|\hat{\bar{\mathbf{s}}}_{n+1}\right\|^2}} + \alpha_{\mathrm{p}}\mathbf{I}\right) \tag{49}$$

$$\hat{\bar{\boldsymbol{\sigma}}}_{n+1} = \hat{\bar{\boldsymbol{\sigma}}}^{\mathrm{tr}}_{n+1} - \lambda\left(\frac{2\,G_0\,\hat{\bar{\mathbf{s}}}_{n+1}}{\sqrt{\beta_{\mathrm{H}}^2 + \left\|\hat{\bar{\mathbf{s}}}_{n+1}\right\|^2}} + 3K_0\alpha_{\mathrm{p}}\mathbf{I}\right) \tag{50}$$

Moreover, since scalar degradation is assumed, the stress is also decomposed by the same eigenvectors as those of the trial effective stress (i.e., $\mathbf{P}$ in Eq. (46)). This means that it can be calculated as:

$$\boldsymbol{\sigma}_{n+1} = \mathbf{P}_{n+1}(1 - D_{n+1})\,\hat{\bar{\boldsymbol{\sigma}}}_{n+1}\mathbf{P}^{\mathrm{T}}_{n+1} \tag{51}$$

It is also worthwhile to mention that by substituting Eqs. (43)-(45) and (50) into the discrete version of plasticity consistency condition (i.e., $\hat{F}(\hat{\bar{\boldsymbol{\sigma}}}_{n+1}, \boldsymbol{\kappa}_{n+1}) = 0$), the following

[Downloaded from ijce.iust.ac.ir on 2026-11-11]

relation is obtained for the consistency parameter, λ:

$$\lambda = \frac{\alpha\,(\bar{I}_1^{\mathrm{tr}})_{n+1} + \sqrt{\frac{3}{2}}\left\|\hat{\mathbf{s}}_{n+1}^{\mathrm{tr}}\right\| + \eta_{n+1}(\hat{\bar{\sigma}}_1^{\mathrm{tr}})_{n+1} - (1-\alpha)c_{n+1}^{\mathrm{c}}}{9K_0\alpha_{\mathrm{p}}\alpha + \frac{\sqrt{6}\,G_0\left\|\hat{\mathbf{s}}_{n+1}\right\|}{\sqrt{\beta_{\mathrm{H}}^2 + \left\|\hat{\mathbf{s}}_{n+1}\right\|^2}} + \eta_{n+1}\left(\frac{2\,G_0(\hat{\bar{s}}_1)_{n+1}}{\sqrt{\beta_{\mathrm{H}}^2 + \left\|\hat{\mathbf{s}}_{n+1}\right\|^2}} + 3K_0\alpha_{\mathrm{p}}\right)} \quad (52)$$

where η is a new function defined as:

$$\eta_{n+1} = \begin{cases} \beta_{n+1} & \text{, IF } (\hat{\bar{\sigma}}_1^{\mathrm{tr}})_{n+1} > 0 \\ \gamma & \text{, Otherwise} \end{cases} \quad (53)$$

Since λ in equation (52) is dependent on $\hat{\bar{\mathbf{s}}}_{n+1}$, it cannot be explicitly computed. Furthermore, λ needs to satisfy Eq. (44). Therefore the consistency parameter is obtained from an iterative strategy using these two relations.

3.3. Stress Calculation Procedure

Computation of stress is based on the classic step by step iterative method which is composed of elastic prediction and plastic-damage correction. During this process, as well as stress, $\sum$, other variables such as $\boldsymbol{\varepsilon}^{\mathrm{p}}$, $\mathbf{k}_{\mathrm{t}}$, $\mathbf{k}_{\mathrm{c}}$, D_t and D_{c} are updated. From an implementation point of view, it is more convenient that D_t and D_{c} are considered as a vector similar to $\mathbf{k}$ (i.e., $\mathbf{D}=(D_{\mathrm{t}}\ \ D_{\mathrm{c}})^{\mathrm{T}}$). The computational procedure for the stress at step *n+1* can be summarized as Table 2.

3.4. Consistent Algorithmic Tangent Stiffness

When the Newton-Raphson algorithm is employed in global iterations, the rate of convergence is strongly dependent on the elastoplastic tangent stiffness. Using the algorithmic tangent stiffness, which is consistent with the local iteration as well, guarantees the quadratic convergence in global iterations [16]. The consistent algorithmic tangent stiffness is defined by combining the linearized equations having been used in the local iteration algorithm derived to compute stresses.

After the converged effective stresses and damage variables are computed for the given strain, all the residual equations, Eqs. (54)-(56), are assumed to be satisfied.

$$\mathbf{Q}(\hat{\bar{\boldsymbol{\sigma}}}_{n+1}, \boldsymbol{\kappa}_{n+1}, \lambda) = \mathbf{0} \quad (54)$$

$$\hat{F}(\hat{\bar{\boldsymbol{\sigma}}}_{n+1}, \boldsymbol{\kappa}_{n+1}) = 0 \quad (55)$$

$$\bar{\boldsymbol{\sigma}}_{n+1} = \mathbf{E}_0 : (\boldsymbol{\varepsilon}_{n+1} - \boldsymbol{\varepsilon}_{n+1}^{\mathrm{p}}) \quad (56)$$

Having equation (54), the total differential of $\mathbf{Q}$ becomes:

$$d\mathbf{Q} = \frac{\partial \mathbf{Q}}{\partial \boldsymbol{\kappa}} \cdot d\boldsymbol{\kappa} + \frac{\partial \mathbf{Q}}{\partial \hat{\bar{\boldsymbol{\sigma}}}} : d\hat{\bar{\boldsymbol{\sigma}}} + \frac{\partial \mathbf{Q}}{\partial \lambda} d\lambda \quad (57)$$

Table 2. Stress calculation procedure for an integration point

0. $\boldsymbol{\varepsilon}_{n+1}$, $\boldsymbol{\varepsilon}_n^{\mathrm{p}}$, $\boldsymbol{\kappa}_n$, $\mathbf{D}_n$
1. $\bar{\boldsymbol{\sigma}}_{n+1}^{\mathrm{tr}} = \mathbf{E}_0 : (\boldsymbol{\varepsilon}_{n+1} - \boldsymbol{\varepsilon}_n^{\mathrm{p}})$
2. $\bar{\boldsymbol{\sigma}}_{n+1}^{\mathrm{tr}} = \mathbf{P}_{n+1}\,\hat{\bar{\boldsymbol{\sigma}}}_{n+1}^{\mathrm{tr}}\,\mathbf{P}_{n+1}^{\mathrm{T}}$
3. IF $\hat{F}(\hat{\bar{\boldsymbol{\sigma}}}_{n+1}^{\mathrm{tr}}, \boldsymbol{\kappa}_n) \le 0$ THEN (*Elastic loading/unloading state*)
   3.1. $\hat{\bar{\boldsymbol{\sigma}}}_{n+1} = \hat{\bar{\boldsymbol{\sigma}}}_{n+1}^{\mathrm{tr}};\ \boldsymbol{\varepsilon}_{n+1}^{\mathrm{p}} = \boldsymbol{\varepsilon}_n^{\mathrm{p}};\ \boldsymbol{\kappa}_{n+1} = \boldsymbol{\kappa}_n;\ \mathbf{D}_{n+1} = \mathbf{D}_n$
4. ELSE (*Plastic loading state*)
   4.1. Return-mapping process (local iteration to compute $\hat{\bar{\boldsymbol{\sigma}}}_{n+1}, \boldsymbol{\kappa}_{n+1}, \lambda$)
   4.2. $\Delta\hat{\boldsymbol{\varepsilon}}^{\mathrm{p}} = \lambda \nabla_{\hat{\bar{\boldsymbol{\sigma}}}} \hat{\Phi}$
   4.3. $\boldsymbol{\varepsilon}_{n+1}^{\mathrm{p}} = \boldsymbol{\varepsilon}_n^{\mathrm{p}} + \mathbf{P}_{n+1}\,\Delta\hat{\boldsymbol{\varepsilon}}^{\mathrm{p}}\,\mathbf{P}_{n+1}^{\mathrm{T}}$
   4.4. $\mathbf{D}_{n+1} = \mathbf{D}(\boldsymbol{\kappa}_{n+1})$
5. $s_{n+1} = s\,(\hat{\bar{\boldsymbol{\sigma}}}_{n+1})$
6. $D_{n+1} = 1 - (1 - D_{n+1}^{\mathrm{c}})(1 - s_{n+1} D_{n+1}^{\mathrm{t}})$
7. $\bar{\boldsymbol{\sigma}}_{n+1} = \mathbf{P}_{n+1}\,\hat{\bar{\boldsymbol{\sigma}}}_{n+1}\,\mathbf{P}_{n+1}^{\mathrm{T}}$
8. $\boldsymbol{\sigma}_{n+1} = (1 - D_{n+1})\,\bar{\boldsymbol{\sigma}}_{n+1}$

[Downloaded from ijce.iust.ac.ir on 2026-11-11]

which is expected to be zero (i.e.,$dQ=0$). Taking this into consideration, the following relation is obtained by rearranging this latter equation:

$$d\boldsymbol{\kappa} = \mathbf{T}_{\boldsymbol{\kappa}\bar{\boldsymbol{\sigma}}} : d\bar{\boldsymbol{\sigma}} + \mathbf{T}_{\boldsymbol{\kappa}\lambda}\, d\lambda \tag{58}$$

where $\mathbf{T}_{\boldsymbol{\kappa}\bar{\boldsymbol{\sigma}}}$ and $\mathbf{T}_{\boldsymbol{\kappa}\lambda}$ would have the following form, respectively:

$$\mathbf{T}_{\boldsymbol{\kappa}\bar{\boldsymbol{\sigma}}} = -\left(\frac{\partial \mathbf{Q}}{\partial \boldsymbol{\kappa}}\right)^{-1} \cdot \frac{\partial \mathbf{Q}}{\partial \hat{\bar{\boldsymbol{\sigma}}}} : \frac{\partial \hat{\bar{\boldsymbol{\sigma}}}}{\partial \bar{\boldsymbol{\sigma}}} \tag{59}$$

$$\mathbf{T}_{\boldsymbol{\kappa}\lambda} = -\left(\frac{\partial \mathbf{Q}}{\partial \boldsymbol{\kappa}}\right)^{-1} \cdot \frac{\partial \mathbf{Q}}{\partial \lambda} \tag{60}$$

Similarly, from Eq. (55) the total differential of function $\hat{F}$ gives:

$$\nabla_{\hat{\bar{\boldsymbol{\sigma}}}} \hat{F} : d\hat{\bar{\boldsymbol{\sigma}}} + \nabla_{\boldsymbol{\kappa}} \hat{F} \cdot d\boldsymbol{\kappa} = 0 \tag{61}$$

Substituting Eq. (58) into Eq. (61), it yields:

$$\mathbf{T}_{\hat{F}\bar{\boldsymbol{\sigma}}} : d\bar{\boldsymbol{\sigma}} + T_{\hat{F}\lambda}\, d\lambda = 0 \tag{62}$$

where $\mathbf{T}_{\hat{F}\bar{\boldsymbol{\sigma}}}$ and $T_{\hat{F}\lambda}$ are defined as below:

$$\mathbf{T}_{\hat{F}\bar{\boldsymbol{\sigma}}} = \nabla_{\hat{\bar{\boldsymbol{\sigma}}}} \hat{F} : \partial \hat{\bar{\boldsymbol{\sigma}}} / \partial \bar{\boldsymbol{\sigma}} + \nabla_{\boldsymbol{\kappa}} \hat{F} \cdot \mathbf{T}_{\boldsymbol{\kappa}\bar{\boldsymbol{\sigma}}} \tag{63}$$

$$T_{\hat{F}\lambda} = \nabla_{\boldsymbol{\kappa}} \hat{F} \cdot \mathbf{T}_{\boldsymbol{\kappa}\lambda} \tag{64}$$

Moreover, based on Eq. (56), the total differential of the stress becomes:

$$d\bar{\boldsymbol{\sigma}} = \mathbf{E}_0 : (d\boldsymbol{\varepsilon} - d\boldsymbol{\varepsilon}^{\mathrm{p}}) \tag{65}$$

in which the total differential of the plastic strain is:

$$d\boldsymbol{\varepsilon}^{\mathrm{p}} = \nabla_{\bar{\boldsymbol{\sigma}}} \Phi\, d\lambda + \lambda\, \partial^2 \Phi / \partial \bar{\boldsymbol{\sigma}}^2 : d\bar{\boldsymbol{\sigma}} \tag{66}$$

By employing equation (66) and defining a modified stiffness $\mathbf{S} = \left(\mathbf{E}_0^{-1} + \lambda\, \partial^2 \Phi / \partial \bar{\boldsymbol{\sigma}}^2\right)^{-1}$, Eq. (65) may be rewritten as:

$$d\bar{\boldsymbol{\sigma}} = \mathbf{S} : d\boldsymbol{\varepsilon} - \mathbf{S} : \nabla_{\bar{\boldsymbol{\sigma}}} \Phi\, d\lambda \tag{67}$$

Substituting Eq. (67) into Eq. (62), one obtains the relation for $\mathrm{d}\lambda$:

$$d\lambda = \left(\frac{\mathbf{T}_{\hat{F}\bar{\boldsymbol{\sigma}}} : \mathbf{S}}{\mathbf{T}_{\hat{F}\bar{\boldsymbol{\sigma}}} : \mathbf{S} : \nabla_{\bar{\boldsymbol{\sigma}}} \Phi - T_{\hat{F}\lambda}}\right) : d\boldsymbol{\varepsilon} \tag{68}$$

which is substituted back into equation (67) to obtain:

$$d\bar{\boldsymbol{\sigma}} = \left(\mathbf{S} - \frac{\mathbf{S} : \nabla_{\bar{\boldsymbol{\sigma}}} \Phi \otimes \mathbf{T}_{\hat{F}\bar{\boldsymbol{\sigma}}} : \mathbf{S}}{\mathbf{T}_{\hat{F}\bar{\boldsymbol{\sigma}}} : \mathbf{S} : \nabla_{\bar{\boldsymbol{\sigma}}} \Phi - T_{\hat{F}\lambda}}\right) : d\boldsymbol{\varepsilon} \tag{69}$$

Furthermore, based on equation (36), the total differential of the stress tensor is written as:

$$d\boldsymbol{\sigma} = -\,\bar{\boldsymbol{\sigma}}_{n+1}\, dD + (1 - D_{n+1})\, d\bar{\boldsymbol{\sigma}} \tag{70}$$

Since the total degradation, D, is a function of $\mathbf{k}$ and $\hat{\bar{\boldsymbol{\sigma}}}$ (i.e., $D_{n+1} = D(\mathbf{D}(\boldsymbol{\kappa}_{n+1}), \hat{\bar{\boldsymbol{\sigma}}}_{n+1})$), the following is concluded:

$$dD = \frac{\partial D}{\partial \mathbf{D}} \cdot \frac{\partial \mathbf{D}}{\partial \boldsymbol{\kappa}} \cdot d\boldsymbol{\kappa} + \frac{\partial D}{\partial \hat{\bar{\boldsymbol{\sigma}}}} : \frac{\partial \hat{\bar{\boldsymbol{\sigma}}}}{\partial \bar{\boldsymbol{\sigma}}} : d\bar{\boldsymbol{\sigma}} \tag{71}$$

Substituting Eq. (58) into Eq. (71) gives the differential of the degradation as:

$$dD = \mathbf{T}_{D\bar{\boldsymbol{\sigma}}} : d\bar{\boldsymbol{\sigma}} + T_{D\lambda}\, d\lambda \tag{72}$$

where the following definitions for $\mathbf{T}_{D\bar{\boldsymbol{\sigma}}}$ and $T_{D\lambda}$ are being employed:

$$\mathbf{T}_{D\bar{\boldsymbol{\sigma}}} = \frac{\partial D}{\partial \hat{\bar{\boldsymbol{\sigma}}}} : \frac{\partial \hat{\bar{\boldsymbol{\sigma}}}}{\partial \bar{\boldsymbol{\sigma}}} + \frac{\partial D}{\partial \mathbf{D}} \cdot \frac{\partial \mathbf{D}}{\partial \boldsymbol{\kappa}} \cdot \mathbf{T}_{\boldsymbol{\kappa}\bar{\boldsymbol{\sigma}}} \tag{73}$$

$$T_{D\lambda} = \frac{\partial D}{\partial \mathbf{D}} \cdot \frac{\partial \mathbf{D}}{\partial \boldsymbol{\kappa}} \cdot \mathbf{T}_{\boldsymbol{\kappa}\lambda} \tag{74}$$

Eq. (70) could lead to the following form by utilizing relation (72):

$$\frac{\partial \boldsymbol{\sigma}}{\partial \boldsymbol{\varepsilon}} = \left[(1 - D_{n+1})\, \mathbf{I} - \bar{\boldsymbol{\sigma}}_{n+1} \otimes \mathbf{T}_{D\bar{\boldsymbol{\sigma}}}\right] : \frac{\partial \bar{\boldsymbol{\sigma}}}{\partial \boldsymbol{\varepsilon}} - T_{D\lambda}\, \bar{\boldsymbol{\sigma}}_{n+1} \otimes \frac{\partial \lambda}{\partial \boldsymbol{\varepsilon}} \tag{75}$$

Employing Eqs. (68) and (69) in Eq. (75), the consistent algorithmic tangent stiffness is concluded:

$$\left(\frac{\partial \boldsymbol{\sigma}}{\partial \boldsymbol{\varepsilon}}\right)_{n+1} = \left[(1 - D_{n+1})\, \mathbf{I} - \bar{\boldsymbol{\sigma}}_{n+1} \otimes \mathbf{T}_{D\bar{\boldsymbol{\sigma}}}\right] : \left(\mathbf{S} - \frac{\mathbf{S} : \nabla_{\bar{\boldsymbol{\sigma}}} \Phi \otimes \mathbf{T}_{\hat{F}\bar{\boldsymbol{\sigma}}} : \mathbf{S}}{\mathbf{T}_{\hat{F}\bar{\boldsymbol{\sigma}}} : \mathbf{S} : \nabla_{\bar{\boldsymbol{\sigma}}} \Phi - T_{\hat{F}\lambda}}\right) - T_{D\lambda} \left(\frac{\bar{\boldsymbol{\sigma}}_{n+1} \otimes \mathbf{T}_{\hat{F}\bar{\boldsymbol{\sigma}}} : \mathbf{S}}{\mathbf{T}_{\hat{F}\bar{\boldsymbol{\sigma}}} : \mathbf{S} : \nabla_{\bar{\boldsymbol{\sigma}}} \Phi - T_{\hat{F}\lambda}}\right) \tag{76}$$

[Downloaded from ijce.iust.ac.ir on 2026-11-11]

It is noted that the derived algorithmic tangent stiffness, Eq. (76), is not symmetric. This is as the result of non-associative flow rule and existence of the degradation component.

4. Numerical Examples

This section describes numerical simulations used to validate the implemented plastic-damage model in its 3-D development. The numerical algorithm discussed above has been implemented in a special finite element program (i.e. SNACS [18]) using a series of FORTRAN subroutines. This part is divided into two subsections including single-element tests and structural application. In all executions, the model parameters of α, γ, α_p, s_0 and $\boldsymbol{\varepsilon}_1$ are equal to 0.12, 3.0, 0.2, 0.0 and 0.1, respectively. Furthermore, in all cases $\tilde{D}_t$=0.51 and $\tilde{D}_c$=0.4 . It should be also mentioned that the displacement control approach is used to apply the loadings.

4.1. Single-element Tests

The implementation is initially validated by applying the model to evaluate the numerical response of several examples for which experimental results are available. Thereafter, the results of some additional numerical tests are presented. The first two verifications discussed here confirm the basic capabilities of the present plastic-damage model in representing tensile and compressive behavior of concrete under monotonic loading. For this purpose, one 8-node isoparametric solid element with 2 x 2 x 2 Gauss integration with l_{ch}=25.4 mm is used. For all cases, unless otherwise specified, the following material properties are utilized:

Table 3. Material properties for the one-element tests

E_0 (GPa)	ν -	f'_t (MPa)	f'_c (MPa)	G_t (N/m)	G_c (N/m)
31.0	0.18	3.48	27.6	12.3	1750

4.1.1. Monotonic Uniaxial Loadings

Performance of the model for the fundamental loadings such as uniaxial tensile and compressive loading tests is evaluated and compared with the corresponding experiments and results from Lee and Fenves by 2-D implementation. It should be mentioned that in the uniaxial compressive case, elastic modulus, E_0 of 31.7 GPa is utilized instead of 31.0 GPa. Fig. 3 depicts the simulated tensile and compressive stress-strain curves, respectively. It is observed that the numerical results agree well with the experimental data and also with the solutions of Lee and Fenves.

4.1.2. Monotonic Biaxial Loadings

To test numerical behavior of the model under biaxial state of stresses, the test results for biaxial

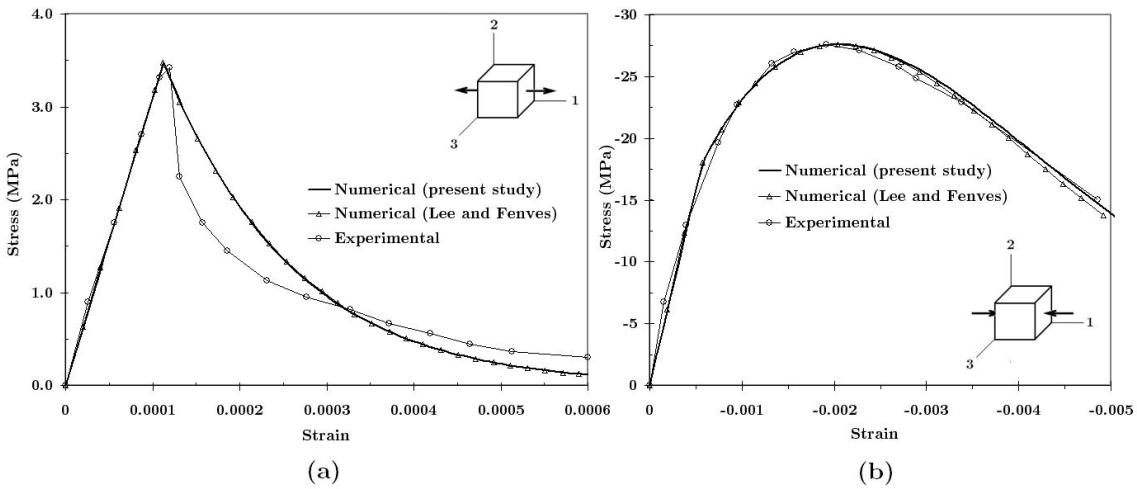

Fig. 3. Monotonic uniaxial loadings compared with experiment [19,20], and also with Lee and Fenves study [9]; (a) tensile test, (b) compressive test

[Downloaded from ijce.iust.ac.ir on 2026-11-11]

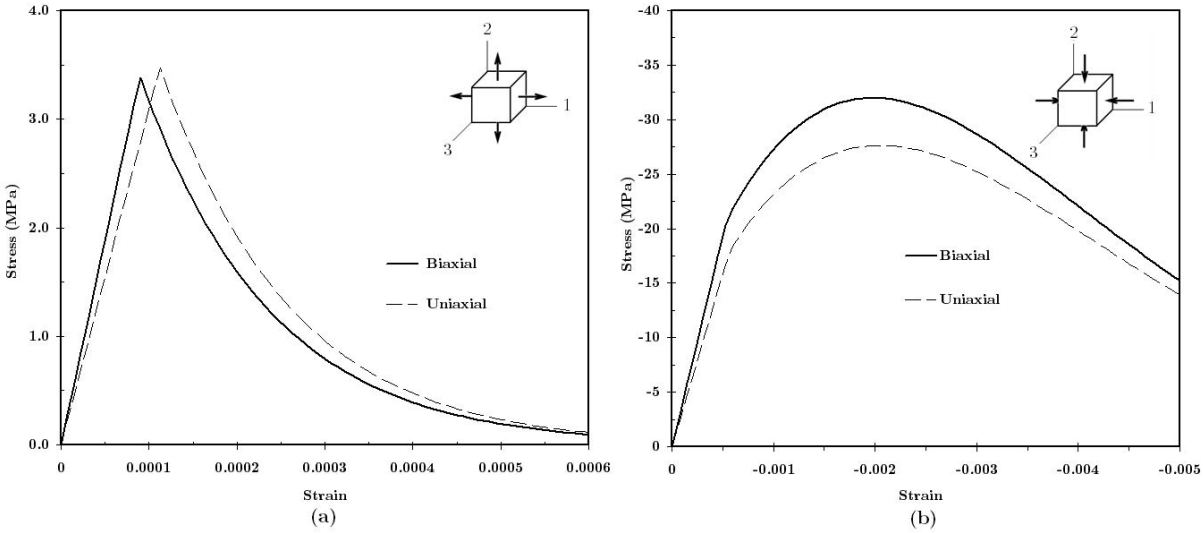

Fig. 4. Biaxial loading tests along with uniaxial responses: (a) tension, (b) compression

tensile case and compressive case are compared with their uniaxial cases in Fig. 4a and 4b, respectively. The same material data considered for uniaxial loading are employed for these cases.

It is noted that as expected, the strength of concrete is predicted to slightly decrease for the biaxial loading in tension, while it shows a significant increase for the biaxial loading in compression.

4.1.3. Triaxial and Constrained Biaxial Tension Tests

In order to evaluate the implemented procedure for the singularity treatment of the apex, two examples including triaxial test and constrained biaxial test are examined in this subsection.

Fig. 5a compares the numerical predictions for triaxial case along with the uniaxial and biaxial results obtained previously. The third direction is restrained in the constrained biaxial test. It is noted that tensile stress develops in that direction as equal tensile strains are exerted in the other two directions. Furthermore, the three tensile stresses become equal at certain stage and remain equal afterwards. From that point forward, states of stresses correspond to the point on the apex of the plastic potential surface. The result of this test (Fig. 5b) demonstrates the capability of the strategy adopted here to overcome this singularity.

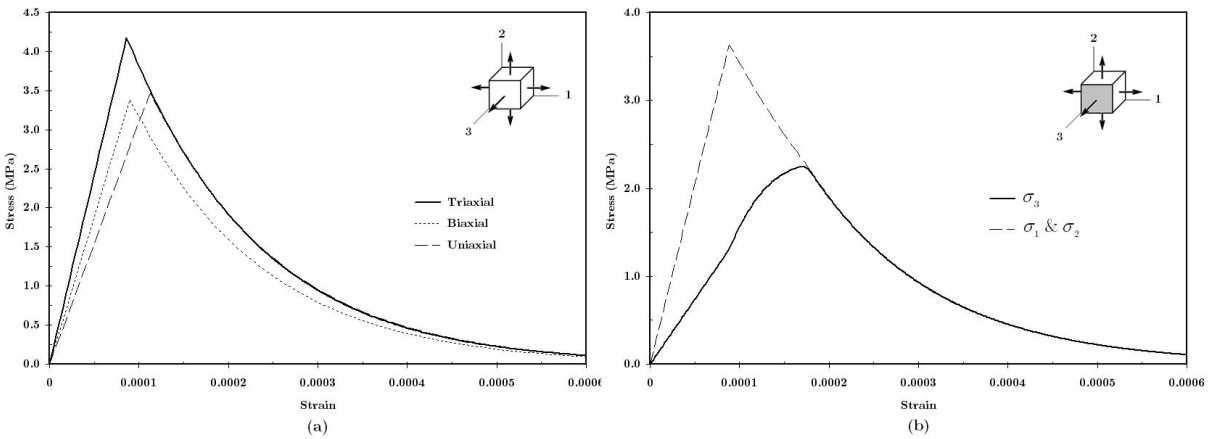

Fig. 5. (a) Uniaxial, biaxial, triaxial tensile loading results; (b) Constrained biaxial test

[Downloaded from ijce.iust.ac.ir on 2026-11-11]

4.1.4. Triaxial Compression Test

As mentioned above, Lubliner's yield function contains a term, γ, which can better predict the concrete behavior in compression under confinement. The numerical results of the present model for this type of loading are compared between the case of γ=0 and γ=3. The material properties adopted in the simulations are the same as used for the uniaxial compression test. The numerical predictions of specimens under three sets of confining stresses, namely, σ_2=σ_3=0.0 MPa, σ_2=σ_3=-3.75 MPa and σ_2=σ_3=-7.50 MPa, are reproduced in Fig. 6. It should be mentioned that the confining stresses are increased proportional to the imposed strain in the third direction for all these cases. It can be clearly seen that the enhancement of strength and ductility due to the compressive confinement are satisfactorily captured by the present model.

4.1.5. Cyclic Uniaxial Loadings

Herein, cyclic loading applications are presented. The main objective is to examine the capability of the model in capturing stiffness degradation in both tensile and compressive loadings. The material properties are the same as those of Table 3 except E_0=31.7 GPa and $\tilde{D}_c$=0.38. Figs. 7a and 7b illustrate the numerical results from two uniaxial cyclic loading cases which are compared against the experimental data in each case.

For both cases, the stiffness degradation is seen to be properly simulated at each unloading/reloading cycle. However, it is noted that hysteresis on reloading cannot be captured by the model because of the rate-independent elastic loading/unloading assumption. It is noted that in some structures the dominant failure mechanism is shear damage [21] which in this plastic-damage model, both damages in tension and compression are expected in such examples.

4.1.6. Full Cyclic Loading

In the last case, the single-element is subjected to cyclic tensile-compressive-tensile load (Fig. 8). This perfectly illustrates the ability of the model to simulate stiffness recovery when the status changes from tension to compression and vice versa. The tensile strength after compressive loading is degraded and it means that the tensile damage and the elastic stiffness are considerably affected by the compressive damage.

4.2. Structural Application

The analysis of a notched concrete beam

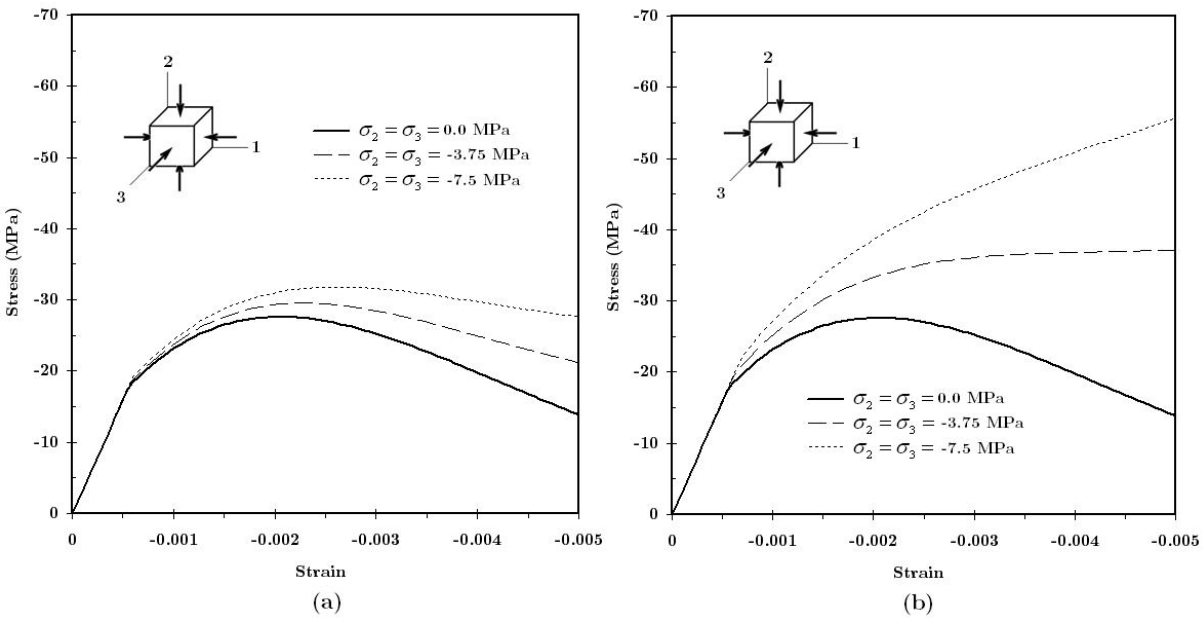

Fig. 6. $\sigma_1 - \varepsilon_1$ curves under three different confinements: (a) $\gamma = 0$ and (b) $\gamma = 3$

[Downloaded from ijce.iust.ac.ir on 2026-11-11]

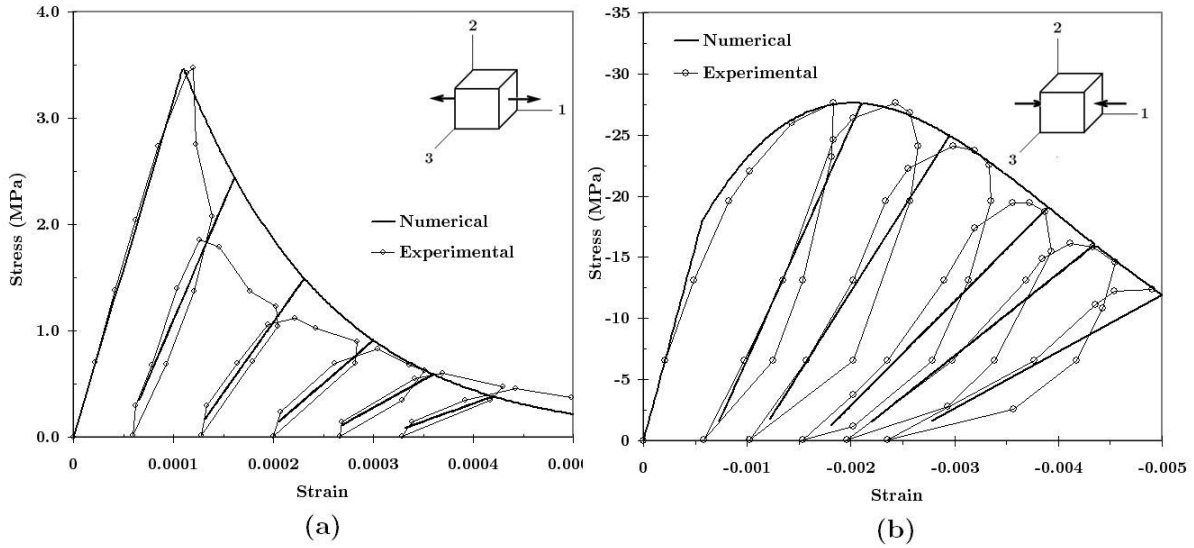

Fig. 7. Cyclic uniaxial loading results in comparison with experimental result [19,20]: (a) tensile test and (b) compressive test

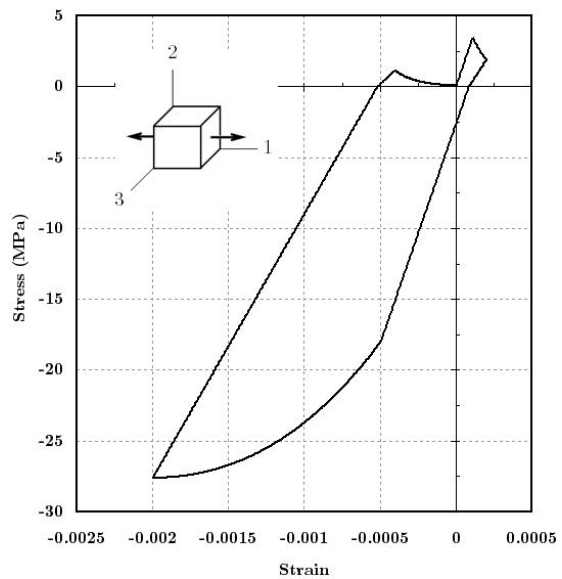

Fig. 8. Numerical solution for full cyclic loading case

monotonically loaded under four-point bending is investigated herein to examine the implemented algorithm in a real 3-D application. This problem has been extensively studied by researchers in both experiments and numerical modeling [22,23]. The specifications of the test are illustrated in Fig. 9a. A 3D 8-node finite element mesh for the symmetric left part of the specimen is also shown in Fig 9b.

The material properties used in this application are defined in Table 4. It should be mentioned that the size of the elements in the expected localization zone is used here as the characteristic length, . To calibrate the material data for the present model, slightly lower values than in the experimental test investigated by Hordijk [22] are assumed for the tensile strength and fracture energy in tension. To evaluate the

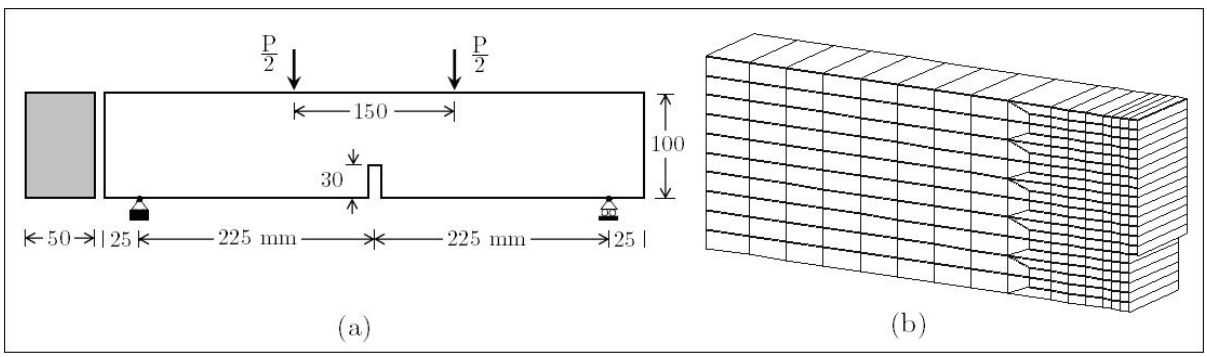

Fig. 9. Four-point bending test: (a) geometry of the specimen and boundary conditions (b) 3D 8-node finite element mesh

[Downloaded from ijce.iust.ac.ir on 2026-11-11]

Table 4. Material properties for the notched beam

E_0 (GPa)	ν -	f_t' (MPa)	f_c' (MPa)	G_t (N/m)	G_c (N/m)
38.0	0.2	2.9	30.0	65.0	6500

accuracy of the solution, three analyses are carried out with different number of increments; these are 15, 30 and 60 equal steps which are considered within the applied maximum displacement.

Fig. 10a shows the load P versus the load point deflection for the numerical simulations and the corresponding experimental test. The three analyses excellently agree with one another, confirming robust convergence of the algorithm and good accuracy of the solution over a large range of displacement increments. The damage development at the end of the analysis is also illustrated in Fig. 10b which is clearly showing the localization in the model.

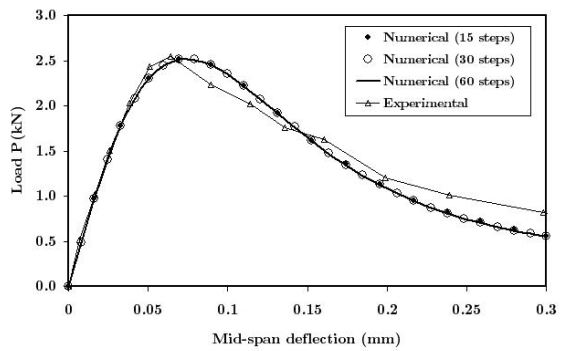

(a)

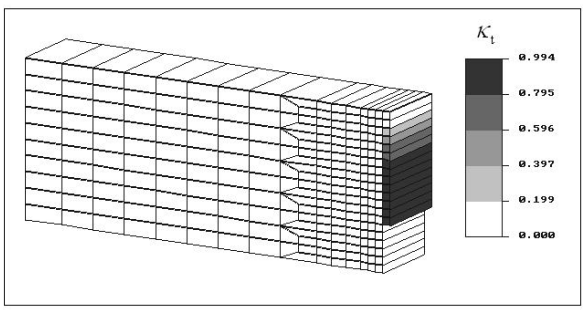

(b)

Fig. 10. Four-point bending test: (a) Load-deflection curves for different number of steps compared with the experiment result [22], (b) Tensile damage at the end of the analysis

5. Conclusions

Constitutive relations of the plastic-damage model proposed by Lee and Fenves are reviewed and its computational aspects in 3-D implementation mainly related to the singularity of the original plastic potential function are discussed in this paper. It should be noted that the implementation and examples carried out by Lee and Fenves were limited to 2-D plane stress problems. In 3-D development, a part of the implementation of the return-mapping process needs to be reformulated due to employing the Drucker-Prager hyperbolic potential function as a treatment for the apex's singularity of the linear one.

The effective stress concept is used to simulate stiffness degradation. The numerical integration is performed by the backward-Euler scheme, which is known to give an unconditionally stable method. The spectral return-mapping which has more advantages with respect to the general return-mapping is utilized. To model dilatancy of concrete accurately, a non-associative flow rule which causes unsymmetrical algorithmic tangent stiffness is used.

Through the numerical examples by several one-element tests, the implemented plastic-damage model is known to give the results that agree well with experimental data for concrete under cyclic loading as well as monotonic loading. It is also demonstrated that stiffness degradation and crack opening/closing are considered properly. In spite of the assumption of isotropy in damage part of the model, this plastic-damage model permits to obtain reliable results in view of the prediction of the failure behavior of concrete. The damage process in a notched beam under four-point bending is investigated numerically, where a comparison is also made with the available experimental result. This real application shows robustness and accuracy of the implemented algorithm in capturing the global softening behavior in concrete structures while it is well representing the expected localization.

References

[1] William, K.J. and Warnke, E.P. (1975), "Constitutive model for the triaxial behavior of concrete", International Association of Bridge

[Downloaded from ijce.iust.ac.ir on 2026-11-11]

and Structural Engineers, Seminar on Concrete Structure Subjected to Triaxial Stresses, Paper III-1, Bergamo, Italy.

[2] Menetrey, Ph. and Willam, K.J. (1995), "Triaxial failure criterion for concrete and its generalization", ACI Structural Journal 92, 311–318.

[3] Grassl, P., Lundgren, K. and Gylltoft, K. (2002), "Concrete in compression: a plasticity theory with a novel hardening law", Int. Journal of Solids and Structures 39: 5205–5223.

[4] Sadrnejad, S.A. and Ghoreishian Amiri, S.A. (2010), "A simple unconventional plasticity model within the multilaminate framework", Int. Journal of Civil Engineering, 8(2): 143-158.

[5] Loland, K.E. (1980), "Continuous damage model for load-response estimation of concrete", Cement & Concrete Research, 10: 395–402.

[6] Mazars, J. and Pijaudier-Cabot, G. (1989), "Continuum damage theory: Application to concrete", Journal of Engineering Mechanics, 115: 345–365.

[7] Lubarda, V.A., Kracjinvovic, D. and Mastilovic, S. (1994), "Damage model for brittle elastic solids with unequal tensile and compressive strength", Engineering Fracture Mechanics 49, 681–697.

[8] Yazdani, S. and Schreyer, H.L. (1990), "Combined plasticity and damage mechanics model for plain concrete", Journal of Engineering Mechanics Division, ASCE, 116: 1435–1450.

[9] Lee, J. and Fenves, G.L. (1998), "A plastic-damage model for cyclic loading of concrete structures", Journal of Engineering Mechanics, ASCE, 124: 892–900.

[10] Gatuingt, F. and Pijaudier-Cabot, G. (2002), "Coupled damage and plasticity modeling in transient dynamic analysis of concrete", Int. Journal of Numerical and Analytical Methods in Geomechanics, 26: 1–24.

[11] Wu, J.U., Li, J. and Faria, R. (2006), "An energy release rate-based plastic-damage model for concrete", Int. Journal of Solids and Structures, 43: 583–612.

[12] Lubliner, J., Oliver, J., Oller, S. and Onate, E. (1989), "A plastic-damage model for concrete", Int. Journal of Solids and Structures, 25: 299–326.

[13] Menzel, A., Ekh, M., Runesson, K. and Steinmann, P. (2005), "A framework for multiplicative elastoplasticity with kinematic hardening coupled to anisotropic damage", Int. Journal of Plasticity, 21(3): 397–434.

[14] Abu Al-Rub, R.K. and Voyiadjis, G.Z. (2003), "On the coupling of anisotropic damage and plasticity models for ductile materials", Int. Journal of Solids and Structures, 40: 2611–2643.

[15] Lee, J. (1996), "Theory and implementation of plastic-damage model for concrete structures under cyclic and dynamic loading", PhD dissertation, Department of Civil and Environmental Eng., University of California, Berkeley, California.

[16] Lee, J. and Fenves, G.L. (2001), "A return-mapping algorithm for plastic-damage models: 3-D and plane stress formulation", Int. Journal for Numerical Methods in Engineering, 50: 487-506.

[17] Simo, J.C. (1992), "Algorithm for static and dynamics multiplicative plasticity that preserve the classical return-mapping schemes of the infinitesimal theory", Computer Methods in Applied Mechanics and Engineering, 99: 61-112.

[18] Omidi, O. (2010), "SNACS: A program for Seismic Nonlinear Analysis of Concrete Structures", Department of Civil and Environmental Eng., Amirkabir University of Technology, Tehran, Iran.

[Downloaded from ijce.iust.ac.ir on 2026-11-11]

[19] Gopalaratnam, V.S. and Shah, S.P. (1985), "Softening response of plain concrete in direct tension" ACI Journal, 3: 310-323.

[20] Karsan, I.D. and Jirsa, J.O. (1969), "Behavior of concrete under compressive loading", Journal of structural division, ASCE, 95(12): 2535-2563.

[21] Arabzadeh, A., Rahaie, A.R. and Aghayari, R. (2009), "A simple strut-and-tie model for prediction of ultimate shear strength of RC deep beams", Int. Journal of Civil Engineering, 7(3): 141-153.

[22] Hordijk, D.A. (1991), "Local approach to fatigue of concrete", PhD dissertation, Delft university of technology, Delft, the Netherlands.

[23] Nguyen G.D. and Korsunsky A.M. (2008), "Development of an approach to constitutive modeling of concrete: isotropic damage coupled with plasticity", Int. Journal of Solids and Structures, 45: 5483-5501.

[Downloaded from ijce.iust.ac.ir on 2026-11-11]